Catalysis Today 164 (2011) 28–33

Contents lists available at ScienceDirect

Catalysis Today

journal homepage: www.elsevier.com/locate/cattod

Selective hydrogenation of 1,3-butadiene over Pd and Pd–Sn catalysts supported on different phases of alumina

Kanda Pattamakomsan[a,b], Eric Ehret[b], Franck Morfin[b], Patrick Gélin[b], Yvette Jugnet[b], Swamny Prakash[b], Jean Claude Bertolini[b], Joongjai Panpranot[a], Francisco José Cadete Santos Aires[b,*]

[a] Center of Excellence on Catalysis and Catalytic Reaction Engineering, Department of Chemical Engineering, Faculty of Engineering, Chulalongkorn University, Bangkok 10330, Thailand

[b] Institut de Recherches sur la Catalyse et l'Environnement de Lyon, UMR 5256 CNRS/Université Lyon1, 2 Avenue Albert Einstein, 69626 Villeurbanne Cedex, France

ARTICLE INFO

Article history:
Available online 13 November 2010

Keywords:
1,3-Butadiene hydrogenation
Pd/Al_2O_3
$Pd–Sn/Al_2O_3$
Mixed phase alumina

ABSTRACT

The gas phase selective hydrogenation of 1,3-butadiene was studied over Pd and Pd–Sn supported on mixed phase θ/α-(MA) and pure α-alumina (AA). The catalysts were characterized by XRD, XPS, TEM, and FTIR spectroscopy of adsorbed CO. A remarkable improvement in terms of activity and selectivity in the selective hydrogenation of 1,3-butadiene was achieved over Pd–Sn on the mixed phase alumina support in which butane formation and isomerization of 1-butene were suppressed. Nevertheless, Pd–Sn/AA showed much lower activity than Pd–Sn/MA due to lower metal dispersion.

1. Introduction

The selective hydrogenation of highly unsaturated hydrocarbons is an important industrial process for purification of petrochemical feedstocks. In this field of research, a challenge is to develop a specific catalyst with the highest selectivity and good stability even at high conversion. Pd catalyst is mostly used in the selective hydrogenation of 1,3-butadiene due to the stronger adsorption of 1,3-butadiene than butenes on Pd surface [1]. Addition of a second metal to Pd catalyst is an efficient way to modify the structural and electronic properties of Pd so that the alkene selectivity is improved [2–4]. Pd based intermetallic compounds and alloys often play an important role in selective hydrogenation reaction [5,6]. Recently, it had been reported that Pd–Sn showed the good selectivity in selective hydrogenation of 1,3-butadiene without coking of the catalyst [7]. Furthermore, the crystalline phase of alumina can also influence on the physicochemical properties and catalytic performance of Pd catalyst in selective hydrogenation reactions [8,9]. Therefore, it is interesting to determine the effect of tin adding on Pd catalyst supported on different alumina phases on the physicochemical properties and catalytic performance. Furthermore, the method of preparation should have the potential to further manufacture a conventional catalyst for industrial application.

In this study, Pd and Pd–Sn catalysts supported on mixed phase θ/α- and pure α-alumina were prepared by impregnation method. Their physicochemical properties were characterized by various techniques such as X-ray diffraction (XRD), photoelectron spectroscopy (XPS), transmission electron microscopy (TEM), and Fourier transform infrared spectroscopy (FT-IR) of chemisorbed CO. The catalytic performance of these catalysts was studied in gas-phase selective hydrogenation of 1,3-butadiene under various reaction conditions.

2. Catalysts preparation

The mixed phase θ/α-alumina (MA: surface area 46 m^2/g, and pore volume 0.2 cm^3/g) and pure α-alumina (AA: surface area 6 m^2/g, and pore volume 0.01 cm^3/g) supports were obtained by calcination of bayerite ($Al(OH)_3$) (Sasol North America Inc.) at 1100 °C and 1200 °C for 3 h respectively.

Pd/Al_2O_3 (0.5 wt%) catalysts were prepared by impregnation of the alumina supports with a solution of palladium (II) acetylacetonate in toluene. Bimetallic catalysts, $Pd–Sn/Al_2O_3$ (0.5 wt% Pd + 0.2 wt% Sn $(Pd/Sn)_{atomic} = 3$) were prepared by co-impregnation of alumina supports with a solution of palladium (II) acetylacetonate and tin (IV) bis(acetylacetonate) dichloride in toluene. After agitation at room temperature for 24 h and evaporation of the excess toluene solvent, the catalysts were put in a vacuum oven at 80 °C for 24 h. The prepared catalysts were decomposed in argon at 500 °C for 2 h, calcined

* Corresponding author at: Institut de Recherches sur la Catalyse et l'Environnement de LyonUMR 5256 CNRS/Université Lyon1, 2 Avenue Albert Einstein. 69626-Villeurbanne cedex. France. Tel.: +33(0)4 72 44 53 03; fax: +33(0)4 72 44 53 99.
E-mail address: francisco.aires@ircelyon.univ-lyon1.fr (F.J.C.S. Aires).

0920-5861/$ – see front matter © 2010 Elsevier B.V. All rights reserved.
doi:10.1016/j.cattod.2010.10.013

in O_2 at 350 °C for 2 h, and reduced in H_2 at 500 °C for 2 h.

3. Catalyst characterization

The XRD patterns were collected using an X-ray diffractometer, SIEMENS XRD D5000, with Cu K_α radiation with a Ni filter in 10–80° 2θ angular regions. The composition of catalysts was determined using an inductively coupled plasma-optical emission spectroscopy (ICP-OES) Activa (Jobin-Yvon). The BET surface area of Al_2O_3 supports were determined by N_2 physisorption using a Micrometritics ASAP 2000 automated system. The particle size and particle size distribution were determined by transmission electron microscopy using a JEOL JEM 2010, operating at 200 kV, equipped with a LaB6 tip, a high resolution pole piece (0.196 nm point resolution), and a Pentafet-LinK ISIS EDX spectrometer (Oxford Instruments). Local chemical composition of the nanoparticles was determined by energy-dispersive X-ray (EDX) spectroscopy.

XPS analysis was performed with a Kratos Axis Ultra DLD spectrometer, equipped with a hemispherical analyzer, and a state of the art delay line detector. A monochromated Al–K_α X-ray source with charge neutralization was used. In order to reduce the sample a reaction chamber coupled to the ultra-high vacuum XPS chamber allowed to heat the samples in H_2 flow at 500 °C for 2 h and then cool down to room temperature before analysis. The samples can thus be transferred for XPS analysis without air contact. The Al 2p line was taken as an internal standard at 73.4 and 73.6 eV for AA and MA respectively. The error in BE measurements was ±0.2 eV for all catalysts.

Surface investigation was performed by *in situ* FT-IR spectroscopies of adsorbed CO. 40 mg of reduced catalysts were deposited directly on the CaF_2 plate. The samples were pretreated as follows: (i) outgassing at room temperature for 15 min to 1.33×10^{-4} Pa, (ii) heating under vacuum from 20 to 500 °C at heating rate 20 °C/min, (iii) reduction under H_2 at 500 °C for 15 min, (iv) outgassing for 30 min, and then cool down to room temperature before introduction of CO 667 Pa at 20 °C. Carbon monoxide temperature program desorption (CO-TPD) was carried out after evacuation at room temperature for 1 h at heating rate 5 °C/min and recorded every 3 min until CO were completely desorbed. IR spectra were recorded using a Fourier-transform Nexus Thermo Nicolet at a resolution of 2 cm^{-1}. CO gas phase absorbance and background were subtracted from all spectra.

4. Reaction study

The selective hydrogenation of 1,3-butadiene was carried out in a fixed bed flow stainless steel reactor at atmosphere pressure. Before reaction, 50 mg of catalyst was reduced *in situ* with hydrogen by heating from room temperature to 500 °C at a heating rate of 5 °C/min. Then the reactor was cooled down in helium to room temperature. The feed flow rate was adjusted to 100 ml/min with automatic flow controller (Brooks Instruments) and composed of 2% 1,3-butadiene, 2% H_2, and balance with helium. The reaction temperature was adjusted in the range 20–70 °C. The feed and product composition were analyzed by a gas chromatograph equipped with an FID detector (Intersat IGC 120 FB, pack column 0.19% Picric Acid on Graphpac(tm)-GC, 80/100, 7 ft × 1/8 in. SS Tubing).

5. Results and discussion

5.1. Catalyst characterization

The Pd and Pd–Sn bimetallic catalysts supported on MA and AA are denoted herein as Pd/MA, Pd–Sn/MA, Pd/AA, and Pd–Sn/AA. According to our previous study [9], the MA alumina consisted of 80 wt% θ-phase and 20 wt% of α-phase alumina while AA was 100 wt% α-phase alumina. The XRD characteristic peaks corresponding to Pd, Pd–Sn intermetallic phase, and SnO_2 could not be detected for all the catalyst samples due probably to low metal loading and/or the very small particle size. Chemical analysis (ICP) showed that Pd wt% of Pd/MA and Pd–Sn/MA were similar at 0.5 wt%. A slightly less Pd content was found on the catalysts supported on AA (~0.3–0.4 wt%). However, Sn wt% for Pd–Sn catalysts on both alumina supports were 0.2% yielding different atomic ratios (Pd/Sn = 3 for Pd–Sn/MA and Pd/Sn = 2 for Pd–Sn/AA).

TEM micrographs illustrating the morphology of Pd and Pd–Sn supported on MA and AA alumina after reduction at 500 °C for 2 h are shown in Fig. 1. The particle size distributions were examined over 250 particles. The nanoparticles supported on MA alumina were for both samples (Pd/MA and Pd–Sn/MA) around 2 nm with all particles fitting in a very narrow range (1–3 nm). The nanoparticles supported on AA alumina are not so homogeneous in size. Indeed we can observe that together with smaller particles (1–3 nm) we also have a distribution of larger particles. These ranges are between 4 and 6 nm for Pd/AA and 4 and 10 nm for Pd–Sn/AA.

EDX analysis was performed on individual particles in the case of the larger ones and on small groups of (3–5) nanoparticles for the smaller particles. These EDX analysis results are shown in Fig. 2 for Pd–Sn/MA and Pd–Sn/AA. The results suggest that alloy nanoparticles with Pd_3Sn stoichiometry were formed for the bimetallic catalysts regardless of alumina support. However the chemical composition of the bimetallic nanoparticles was much more homogeneous on MA alumina than on AA alumina in which the size distribution was larger. For Pd–Sn/MA we could never detect Sn that was not associated with Pd which strongly suggests that no tin or tin oxide nanoparticles were formed independently of the bimetallic nanoparticles. Conversely, we cannot rule out the possibility of the presence of independent Sn species on the support for Pd–Sn/AA.

The surface composition and electronic properties of Pd and Sn on the various alumina supported Pd and Pd–Sn catalysts were investigated by XPS. The XPS spectra for Pd 3d of all the catalysts after reduction at 500 °C in hydrogen for 2 h are shown in Fig. 3(a). The binding energy of Pd $3d_{5/2}$ is in the range of 334.9–335.3 eV, indicating the presence of metallic palladium species [5]. For the Pd monometallic supported on MA and AA, the binding energy of Pd $3d_{5/2}$ were similar with a maximum at 334.9 eV, indicating that the phase of alumina and Pd particle size had no influence on the electronic property of palladium catalysts [9]. However, the binding energy of Pd $3d_{5/2}$ for Pd–Sn bimetallic on both alumina supports is slightly shifted towards higher binding energy with a maximum at 335.3 eV suggesting that tin addition modifies the electronic properties of Pd catalysts and that bimetallic alloy particles are formed. The deconvoluted XPS spectra of Sn $3d_{5/2}$ for Pd–Sn/MA and Pd–Sn/AA are shown in Fig. 3(b). Both catalysts show two similar components of tin species. The higher binding energy (486.4–486.7 eV) could be related to 32–33 wt% of tin oxide remaining even if the catalysts were reduced in hydrogen flow at 500 °C for 2 h. This observation together with the fact that no Sn was found without Pd by EDX suggests that the remaining unreduced tin is within the bimetallic nanoparticles. On the other hand, 67–68 wt% of tin component observed at the lower binding energy in the range 484.8–484.9 eV could be assigned to the presence of tin alloy [10].

The IR spectra of adsorbed CO 667 Pa at room temperature (Fig. 4) and the IR spectra of CO desorbed at different temperatures in vacuum (not given here) were investigated to further characterize the catalysts and determine the adsorption strength and adsorbed species on Pd and Pd–Sn catalysts supported on MA and AA.

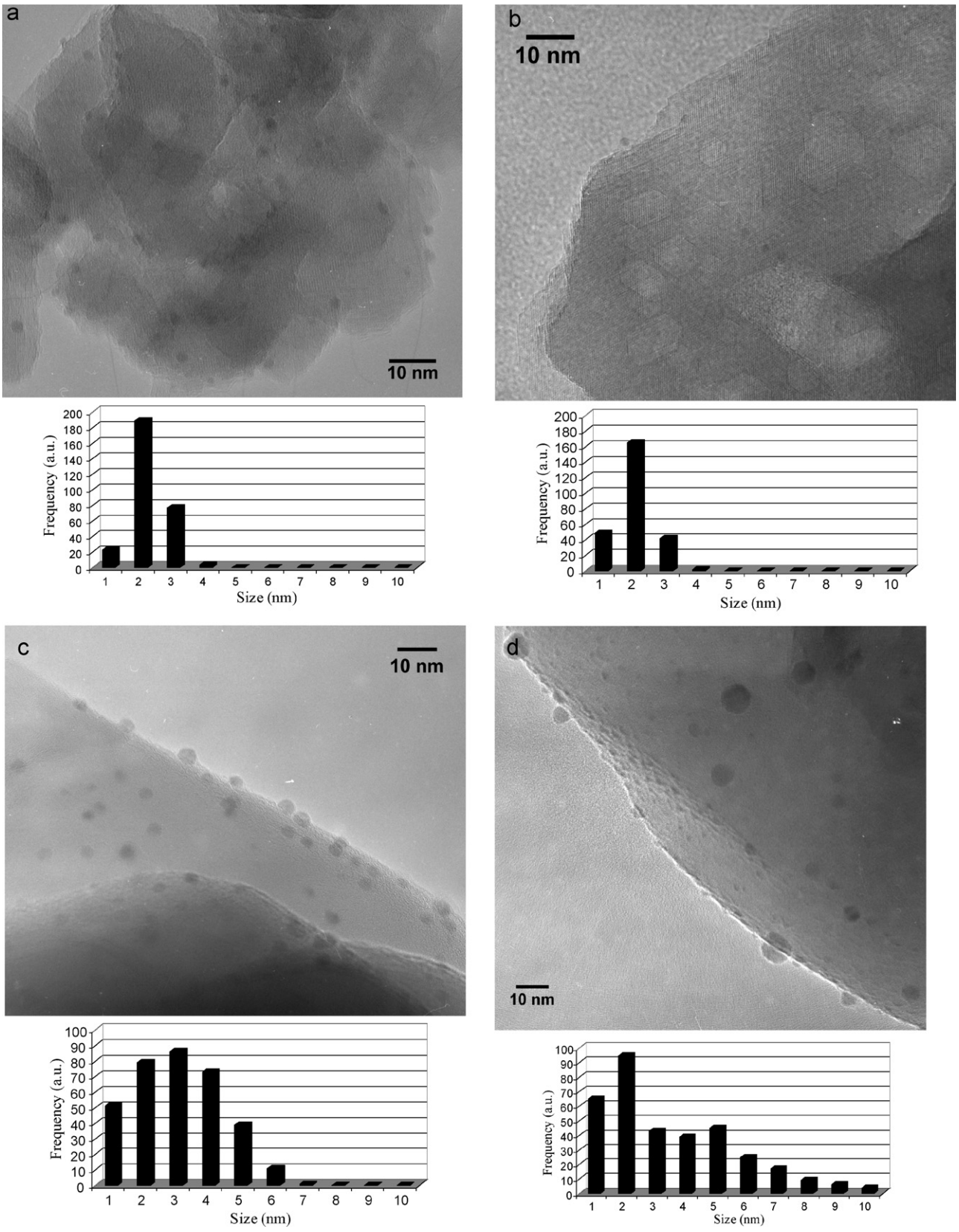

Fig. 1. TEM micrographs of Pd and Pd–Sn catalysts on different alumina supports: (a) Pd/MA, (b) Pd–Sn/MA, (c) Pd/AA, (d) Pd–Sn/AA.

Let us first consider the monometallic catalysts. According to the literature [11–16], the peaks observed in CO–IR results correspond to various CO species adsorbed on metallic Pd, The linear CO species (L) were observed at around 2100 cm^{-1}, and IR band below 2000 cm^{-1} were ascribed to the bridge CO species (B) consisting of isolated bridged species, but also to compressed bridged species interacting with linear CO species and compressed bridge species. In addition, a weak band at around 2200 cm^{-1} (A) is observed for

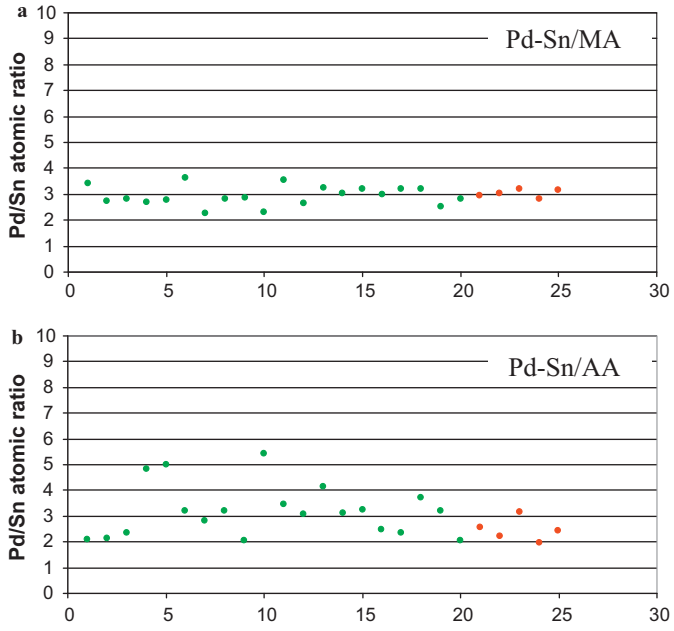

Fig. 2. EDX results for Pd–Sn/MA (a) and Pd–Sn/AA (b) catalysts. Green dots correspond to the EDX analysis of individual nanoparticles or of small group (3–5) nanoparticles. Red dots correspond to the EDX analysis of large regions (~1 μm^2). (For interpretation of the references to color in this figure legend, the reader is referred to the web version of the article.)

adsorbed CO at room temperature on Pd/MA indicating that some CO interacts with Al^{3+} on alumina surface [12,17]. For Pd/MA, the intensity ratio between L and B is equal to 0.5, while bridge bonded species dominate for the Pd/AA catalyst. This is in agreement with the presence of (1 1 1) and (1 0 0) facets actually present on larger nanoparticles for catalysts having a lower dispersion [14–16]. After evacuation 60 min at room temperature, linear species drastically decreased obtaining 2 components, while the bridge species was still constant. The 2 components of linear species may be due to CO interacting with Pd atoms located on different sites, (facets, edges and corners) [11,18,19]. Moreover, temperature program desorption of CO showed that the amount of CO adsorbed decreased when the temperature increased and totally disappeared at 400 °C. In addition, a shift towards lower wave numbers of bridge bonded species during increasing temperature suggests that CO interaction between linear and compressed bridge species are removed [19].

For Pd–Sn/AA and Pd–Sn/MA, both linear and bridge species are observed (Fig. 4). However, the band characteristic of linear species is found at lower wave number (~2090 cm^{-1}), and the intensity ratio between L and B is more important than in the case of monometallic catalysts. This is probably the consequence of some dilution affect associated with the formation of an alloy. The shift of the IR band associated with linear species again suggests that Pd alloy was formed [19]. Moreover, CO-TPD results showed that adsorbed CO was completely removed at 200 °C, and 300 °C for Pd–Sn/AA and Pd–Sn/MA respectively, a sign of electronic interaction of tin on Pd surface atoms.

5.2. Hydrogenation of 1,3-butadiene

The catalytic performance of Pd and Pd–Sn catalysts supported on MA and AA were investigated in the selective hydrogenation of 1,3-butadiene at 30–70 °C and atmospheric pressure. Fig. 5(a) presents the relationship between the conversion of 1,3-butadiene and temperature for all the catalysts. It was found that the conversion of these catalysts were ranged between 5 and 80% and

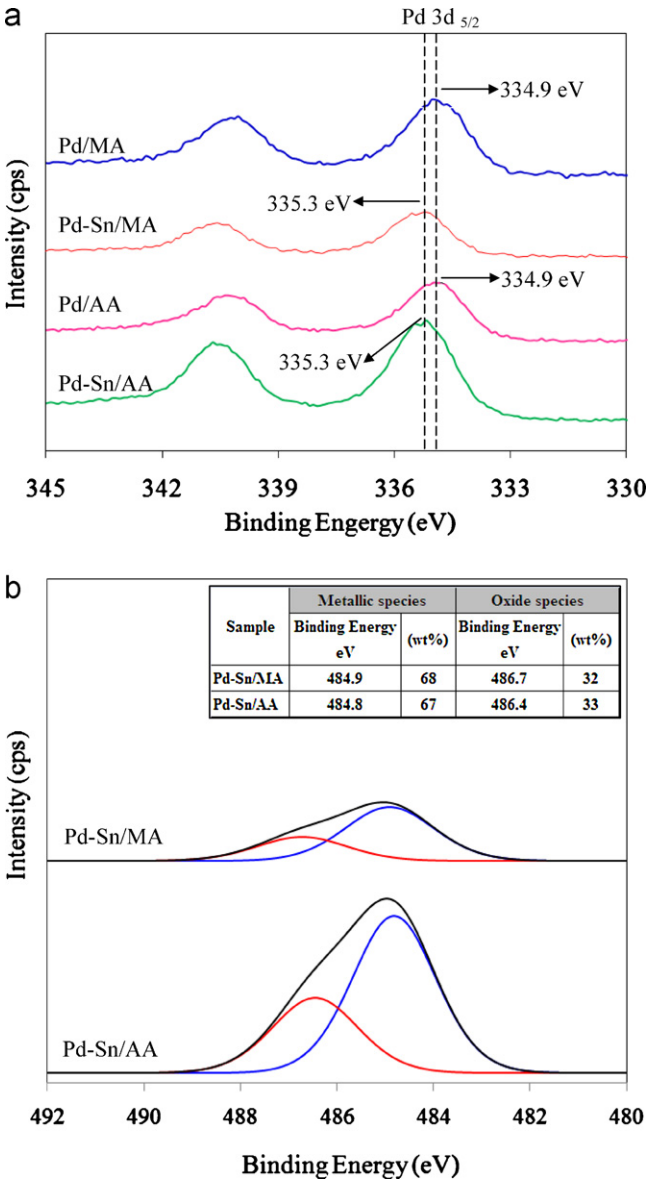

Fig. 3. The deconvoluted XPS spectra (a) Pd 3d$_{5/2}$ and (b) Sn 3d$_{5/2}$.

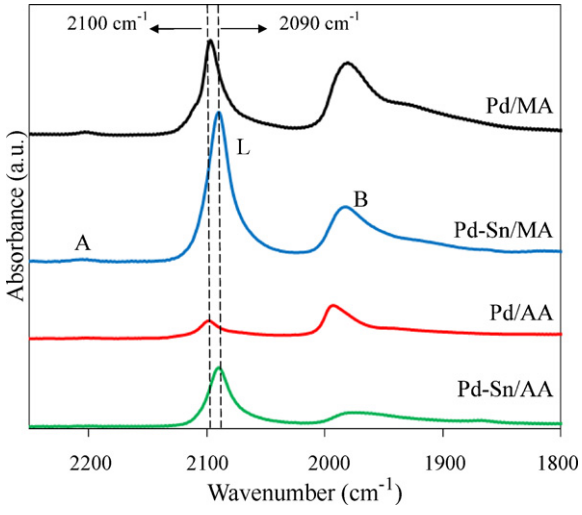

Fig. 4. FTIR spectra of adsorbed CO 667 Pa at room temperature on Pd/MA, Pd–Sn/MA, Pd/AA and Pd–Sn/AA.

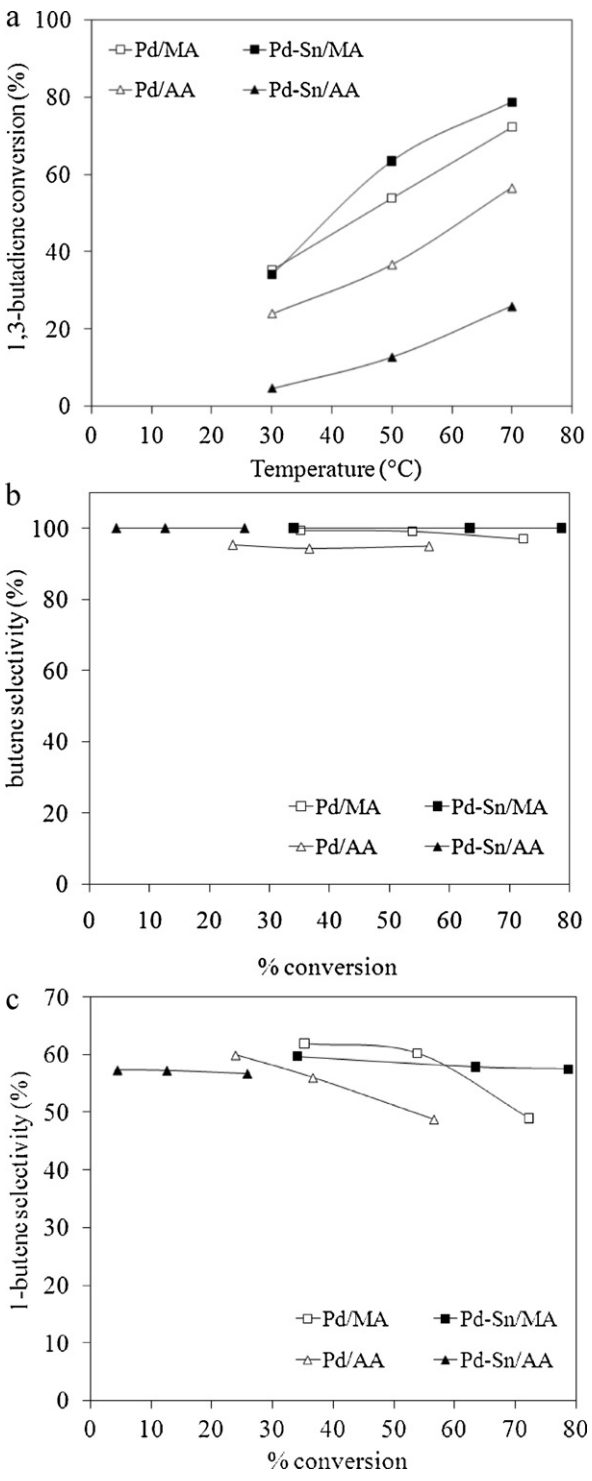

Fig. 5. Catalyst performances in the gas-phase selective hydrogenation of 1,3-butadiene: (a) 1,3-butadiene conversion (%), (b) butene selectivity (%), (c) 1-butene selectivity (%) based on (1 + 2-butenes).

increased with increasing reaction temperature. On mixed alumina support, the turnover frequency (TOF) for Pd and Pd–Sn catalysts are very similar, in range 0.3–0.7 s^{-1}. Conversely on α-alumina we observed a noticeable decrease of TOF for Pd–Sn catalyst (respectively 0.6–1.3 s^{-1} for Pd and 0.1–0.5 s^{-1} for Pd–Sn). The Pd–Sn/MA showed the highest conversion, reaching ~80% at 70 °C. The catalyst activity were in the order Pd–Sn/MA > Pd/MA > Pd/AA > Pd–Sn/AA. For the monometallic Pd catalysts, Pd/MA shows higher activity than Pd/AA due to higher Pd dispersion [9,20,21]. On the MA support, the Pd–Sn/MA was more active than the Pd/MA probably in relation with the increase of the linear/bridge ratio of adsorbed CO on Pd–Sn/MA. Indeed, it had been proposed that CO linear species are preferentially adsorbed on edge and corner, sites on which hydrogenation reaction takes place [17,22–24]. The comparison between Pd–Sn supported on different supports shows that Pd–Sn/AA was much less active than Pd–Sn/MA probably due to the more inhomogeneous particle composition associated with lower % dispersion and/or dilution of Pd coverage on the surface resulting in a lower amount of metal active sites to hydrogenate 1,3-butadiene. The relationship between % butenes selectivity and % conversion of 1,3-butadiene for all the catalysts are presented in Fig. 5(b). It can be seen that Pd/MA and Pd/AA exhibited similar % butenes selectivity (~94–99%). For the Pd–Sn catalysts, butane formation was not observed for the whole range of 1,3-butadiene conversion in this study. It is suggested that butane formation was suppressed by the addition of tin, either via modification of the electronic properties revealed by XPS and CO–IR, inducing a reduction of adsorption strength and/or via the dilution effect of Pd surface atoms by tin. In Fig. 5(c) the 1-butene selectivity with respect to 1 + 2-butenes is plotted versus the 1,3-butadiene conversion over all catalysts. It can be seen that for the monometallic Pd catalysts supported on MA and AA, 1-butene selectivity decreased as the conversion of 1,3-butadiene increased, suggesting that 1-butene isomerization occured at high conversion of 1,3-butadiene. At higher 1,3-butadiene conversion, there was a higher amount of 1-butene product which can adsorb on Pd surface resulting in 1-butene isomerization and/or 1-butene hydrogenation. Interestingly, the isomerization of 1-butene was hindered with using Pd–Sn bimetallic catalysts, especially on the MA support even at high 1,3-butadiene conversion (~80%). The presence of Sn on Pd/alumina induces electronic modification and site dilution effect, which modify the adsorption equilibrium between 1-3-butadiene and butenes and/or may suppress (or at least strongly reduce) isomerization sites on Pd catalysts [24].

6. Conclusions

The Pd and Pd–Sn catalysts supported on mixed θ/α-phases and pure α-phase Al_2O_3 were investigated in the gas phase selective hydrogenation of 1,3-butadiene under various reaction conditions. For the monometallic Pd catalysts, butane was formed and 1-butene was isomerized at high conversion of 1,3-butadiene. In contrast, the bimetallic Pd–Sn catalysts, especially Pd–Sn/MA showed 100% butene selectivity at the relatively high 1,3-butadiene conversion (~80%) without any loss of 1-butene to butane (via hydrogenation) or 2-butene (via isomerization). According to CO–IR results, tin addition played an important role in modifying the nature of surface sites and their electronic properties. However, on the AA support tin addition resulted in a lower Pd dispersion and much lower activity in the selective 1,3-butadiene hydrogenation.

Acknowledgements

The authors would like to thank the Thailand Research Fund (TRF) and the SCG Chemicals Co., Ltd., Thailand for the financial supports for K.P. (contract number IUG50K0002). The authors also would like to thank to Dr. Michael P. Keung, Sasol North America, Inc. for the bayerites used in this study.

References

[1] S. Hub, L. Hilaire, R. Touroude, Appl. Catal. 36 (1988) 307–322.
[2] J.P. Boitiaux, J. Cosyns, M. Derrien, G. Leger, Hydrocarbon Process 64 (1985) 51–59.
[3] R. Ohnishi, H. Suzuki, M. Ichikawa, Catal. Lett. 33 (1995) 341–348.
[4] J. Goetz, M.A. Volpe, C.E. Gigola, R. Touroude, J. Catal. 199 (2001) 338–345.

[5] F.S. Verdier, B. Didillon, S. Morin, D. Uzio, J. Catal. 218 (2003) 288–295.
[6] J. Osswald, K. Kovnir, M. Armbruster, R. Giedigkeit, R.E. Jentoft, U. Wild, Y. Grin, R. Schlogl, J. Catal. 258 (2008) 219–227.
[7] S. Komhom, O. Mekasuwandumrong, P. Praserthdam, J. Panpranot, Catal. Commun. 10 (2008) 86–91.
[8] C. Breinlich, J. Haubrich, C. Becker, A. Valcarcel, F. Delbecq, K. Wandelt, J. Catal. 251 (2007) 123–130.
[9] K. Pattamakomsan, K. Suriye, S. Dokjampa, N. Mongkolsiri, P. Praserthdam, J. Panpranot, Catal. Comm. 11 (2010) 311–316.
[10] J. Arana, P. Ramirez de la Piscina, J. Llorca, J. Sales, N. Homs, J.L.G. Fierro, Chem. Mater. 10 (1998) 1333–1342.
[11] N. Sheppard, T.T. Nguyen, Adv. IR Raman Spectrosc. 5 (1978) 67–148.
[12] D. Tessier, A. Rakai, F. Bozon-Verduraz, J. Chem. Soc. Faraday Trans. 88 (1992) 741–749.
[13] P. Gélin, A.R. Siedle, J.T. Yates Jr., J. Phys. Chem. 88 (1984) 2978–2985.
[14] H.J. Freund, J. Lubuda, M. Baumer, T. Risse, A. Carlsson, Chem. Rec. 3 (2003) 181–201.
[15] F.J. Cadete Santos Aires, G. Garcia Cervantes, J.C. Bertolini, Catal. Lett. 129 (2009) 266–272.
[16] F.J. Cadete Santos Aires, J.C. Bertolini, Top. Catal 52 (2009) 1492–1505.
[17] G. Della Gatta, B. Fubini, G. Ghiotti, C. Morterra, J. Catal. 43 (1976) 90–98.
[18] C. Binet, A. Jadi, J.C. Lavalley, J. Chim. Phys. 86 (1989) 451.
[19] E.A. Sales, J. Jove, M. Mendes, F. Bozon-Verduraz, J. Catal. 195 (2000) 88–95.
[20] A. Sarkany, G. Stefler, J.W. Hightower, Appl. Catal. A 127 (1995) 77–92.
[21] T. Matsuda, M. Sugimoto, React. Kinet. Catal. Lett. 44 (1991) 69–73.
[22] J. Goetz, M.A. Volpe, A.M. Sica, C.E. Gigola, R. Touroude, J. Catal. 167 (1997) 314–323.
[23] L.L. Sheu, Z. Karpinski, W.M.H. Sachtler, J. Phys. Chem. 93 (1989) 4890–4894.
[24] J. Goetz, M.A. Volpe, R. Touroude, J. Catal. 164 (1996) 369–377.